Carbon nanostructures produced through ion irradiation

YU Li-Ping, WANG Zhen-Xia, ZHU Zhi-Yuan, ZHANG Hu-Yong, HAN Jia-Guang, ZHANG Wei, SUN Li-Tao, WANG Ting-Tai, MA Yu-Gang

(Shanghai Institute of Nuclear Research, the Chinese Academy of Sciences, Shanghai 201800)

Abstract Several nanostructures we produced by ion irradiation have been reviewed in this paper. By using ions to irradiate two ultrahigh molecular weight polyethylene targets respectively, it was found that small fullerenes C_{20} and C_{26} were grown, adding two members to the fullerene family. Meanwhile, crystalline diamonds also have been produced by Ar^+ ions irradiation of graphite. In the experiment of double ions Ni^+ and Ar^+ irradiation, nanoscale argon bubbles formed. On the other side, when multi-wall carbon nanotubes were irradiated by C^+, many MWCNTs evolved to amorphous carbon nanowires and amorphous carbon nanotubes. And there are possible welding in the crossed nanotubes.

Keywords Ion irradiation, Nanotube, Fullerenes, Nanocrystalline diamond

CLC numbers O469, O483

1 Introduction

The discovery of fullerene C_{60} and carbon nanotubes aroused great interest in the research community on carbon nanostructures, especially like nanotubes and fullerenes. Understanding electrical and mechanical properties of these nanostructures and exploring their vast applications have a main driving force for this area. The full potential of nanotubes or fullerenes for applications will not be realized until the growth of them can be optimized and well controlled. Up to the present, various methods including arc-discharge, laser ablation, chemical vapor deposition (CVD) and ion irradiation have been developed to grow nanotubes, fullerenes and other nanostructures. Nevertheless, many challenges remain in this area. First, the control over the growth of carbon nanotube as molecular electronic device and the approach to connecting nanometer wires are still lacking. Second, large-scale synthesis of carbon nanostructures such as nanotubes and small fullerenes composed of less than 60 carbon atoms, should be realized. Third, the research on other new carbon nanostructures is little and needs to be carried on further and extensively. Finally, there is a seemly formidable task of understanding clearly the growth mechanism of nanostructures and phase transition by any existing growth models.

Here we reported some results on the growth of carbon nanostructures such as fullerenes, nanocrystalline diamond, nanotubes, argon bubbles, and amorphous carbon nanowires by means of ion-irradiation, which are quite helpful to further understand the mechanisms of their growth and will have great potential applications.

2 Fullerenes C_n(n<60)

The connection between carbon nanotubes and fullerenes was further promoted by the observation that the terminations of the carbon nanotubes were fullerene-like caps or hemispheres. The smallest reported diameter for a carbon nanotube is the same as the diameter of the C_{60} molecules, which is the smallest fullerene to follow the isolated pentagon rule. However, there is not, as yet, a definite answer to this provocative question that whether the minimum diameter of a carbon nanotube is the diameter of C_{60}. Previously, though most work on fullerenes focused on C_{60} and larger fullerenes, the discovery of C_{36} in 1998 showed that C_{60} is not the minimum cage fullerene. And a recent report on a nanotube with the diameter of 0.4 nm and a C_{20} end cap may provide another

Supported by the Major Project of Knowledge Innovation of the Chinese Academy of Sciences (No.KJCX2-SW-N02)

Received date: 2002-08-14

answer to this question. Now, by using ion beam irradiation method, we synthesized C_{20} solids[1,2] and C_{26} crystals[3] respectively, adding two smaller members to the fullerene family experimentally.

2.1 C_{20}

The target material was an ultrahigh molecular weight polyethylene (UHMWPE, -[CH_2]-) block cut from bulk. After being cleaned in acetone, ethanol and deionized water in turn, then air-dried, the target sample surface was irradiated by 60 keV mass-analyzed Ar^+ ions obtained from an electromagnetic isotope separator at the fluence of 10^{18} cm^{-2}. After irradiation, this sample was analyzed by means of transmission electron microscope (TEM), laser desorption past-ionization time-of-flight (TOF) mass spectrometer and Raman spectroscope.

According to the hexagonal array pattern of the first-order diffracted spots (see Fig.1) which suggests a close-packing arrangement, the *d* spacing is 0.46 nm. Assuming that the C_{20} molecule formed into crystal has 12 pentagonal faces, the diameter of such dodecahedron caged structure is calculated to be about 0.31 nm. Therefore, from its magnified HRTEM image and electron diffraction pattern in Fig.1, we believe that C_{20} molecules behave approximately as spheres stacked in the close-packed planes and for such structure of C_{20} molecule crystal the intermolecular bond length of about 0.15 nm can be deduced. This is suggestive of a strong crystal bonding.

We applied TOF test to two prepared samples, one was irradiated by ions while the other was not, in case that potential fullerenes were generated by high-energy laser ablation of UHMWPE. As a result, C_{20} and other fullerenes were not detected in the unirradiated sample. However, the TOF test of ion-irradiated sample, under the same conditions, showed a strong peak at 252 atomic mass units, corresponding to the hydrogen-passivated $C_{20}H_{12}$ molecules of pure C_{20} (see Fig.2), which proved that it was ion irradiation, not laser ablation, that produced fullerenes.

In the typical Raman spectrum (see Fig.3) from the irradiated surface, there are a shoulder peak at 1580 cm^{-1} (G-band) and a low intensity broad peak centered at about 1358 cm^{-1} near Raman peak of diamond at 1332 cm^{-1} (D-band). As reported previously, the existence of G-band for carbon material arises from vibrations of all sp^2 sites, and D-band arises only from cluster of sp^2 sites in six-fold aromatic rings.[4] Since there is a peak at 1358 cm^{-1} very close to the Raman line at 1355 cm^{-1}, the broad D-band might also be explained as the dodecahedron $C_{20}H_{20}$ Raman-active lines. And rich hydrogen in the irradiated surface would also render the constructive Raman band at about 1355 cm^{-1}. So the observation of this D-band in Raman spectrum gives an important hint for the dodecahedron C_{20} cage found in the bombarded surface of PE sample. On the other hand, the unconspicuous peak at about 1469 cm^{-1} on the left of the G-band can also help to confirm the appearance of dodecahedron C_{20} because this 1469 cm^{-1} peak can not be associated with the diamond phase whose structure does not allow any first-order Raman modes higher than 1332 cm^{-1} even in the presence of disorder. Moreover, this peak had been reported in carbon films grown by pulsed laser evaporation of graphite where it was assigned to five-carbon rings,[5] and showed up strongly in fullerenes.[6]

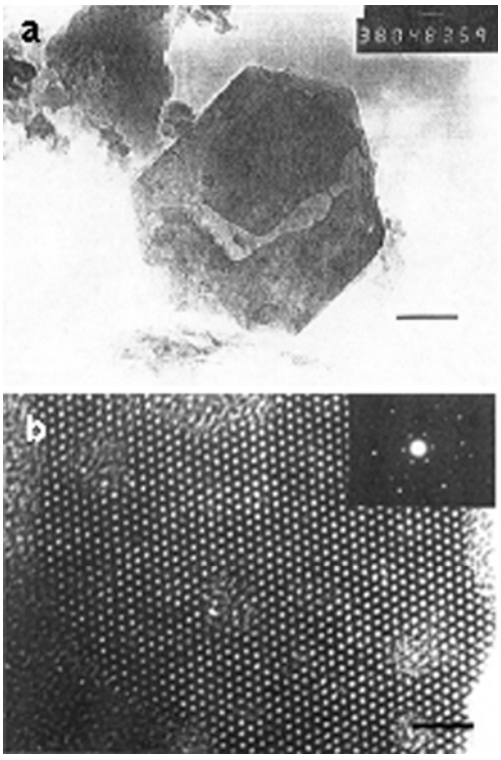

Fig.1 TEM images of C_{20} crystallite in irradiated UHMWPE sample. (a) Low magnification image of C_{20} crystallite with rough hexagonal symmetry. The scale bar is 94 nm. (b) HRTEM image of C_{20} crystallite. The inserted electron diffraction pattern is hexagonal with a calculated *d*-spacing of 0.46 nm. The scale bar is 2 nm.

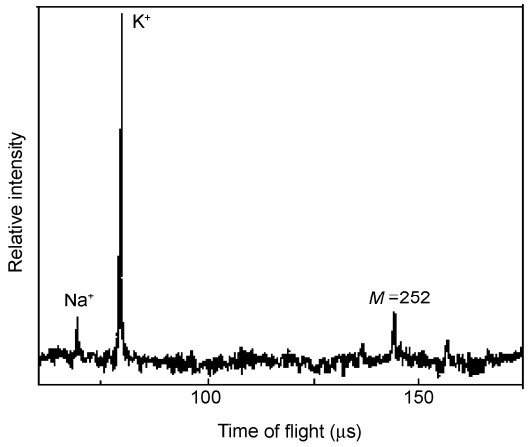

Fig.2 Laser desorption TOF mass spectrum for the irradiated UHMWPE sample showing a strong peak for M = 252 u corresponding to $C_{20}H_{12}$.

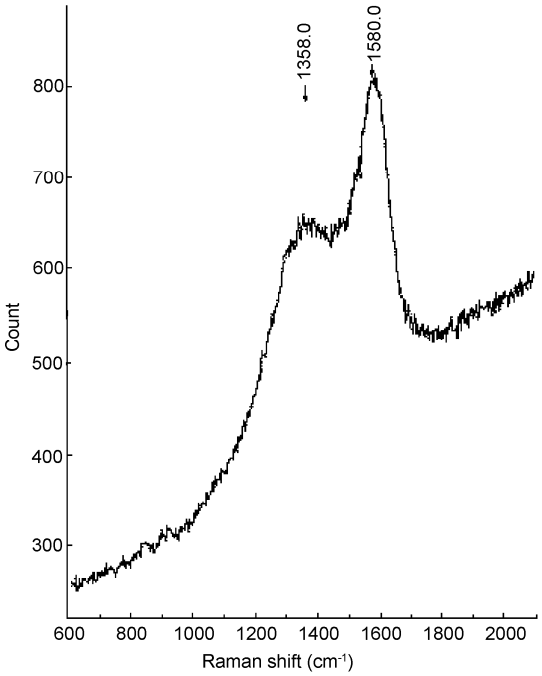

Fig.3 Raman spectrum of Ar^+ irradiated UHMWPE sample.

2.2 C_{26}

Another new form of carbon solid consisting of hexagonal close packing of C_{26} molecules was synthesized by C_2^+ (2.4 MeV, fluence $\sim 5\times10^{16}$ cm^{-2}) ion bombardment in UHMWPE. The experiment process was similar to the above except that C_2^+ ions used here came from a tandem accelerator (1.7×2 MV). The ion beam current was about 150 nA and the residual gas pressure in the irradiation chamber was 1.3×10^{-4} Pa during bombardment. HRTEM, electron diffraction, and TOF mass spectroscope used in the study of molecular packing confirmed that C_{26} molecules have the caged fullerene structure.

The roughly hexagonal crystallite reaches a size of micron quantity. Like its HRTEM image in Fig.4, the electron diffraction spots were composed of regular hexagons similar to those of C_{20} and C_{60} crystal. From these first-order diffracted spots array, the calculated d spacing was about 0.47 nm, suggesting a close-packing arrangement. Similarly, in order to exclude the possibility of forming C_{26} during TOF test, both bombarded UHMWPE surface and un-bombarded surface (inverse surface of the same sample) were tested by the TOF mass spectroscope. There was no any obvious peaks occurred for the un-bombarded surface, while for the bombarded area, there were three conspicuous peaks appearing in the TOF mass spectrum at 438, 554 and 572 amu, possibly corresponding to $C_{26}H_{12}$, $C_{36}H_8$ and $C_{38}H_2$, respectively (see Fig.5). Besides C_{26}, it was shown that C_{36}, which Piskoti *et al* had found in the carbon soot produced by arc-discharge in 1998, could also be produced in this experiment. For C_{38}, there is no direct research work on it up to now, though Zhang *et al*[7] also found it exist in the TOF spectrum of laser irradiating graphite and Kroto also showed its presence clearly in Fig.5 of his paper.[8] So it will be interesting and necessary to further study these smaller fullerenes like C_{36} and C_{38}. Combined with TEM and ED here, only cage-like C_{26} can explain the phenomenon in this experiment. So we think this kind of crystallite was composed of cage C_{26} molecules.

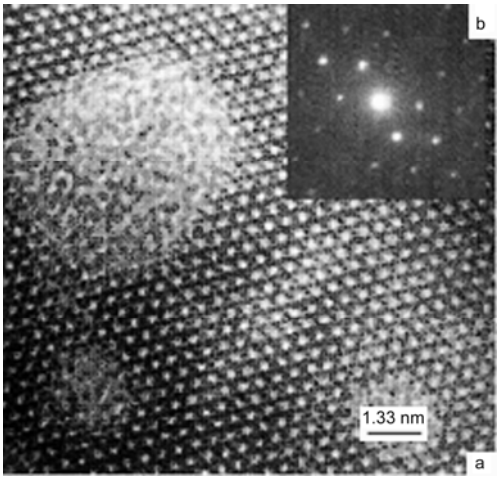

Fig.4 HRTEM image of C_{26} crystallite (a) and its electron diffraction (b).

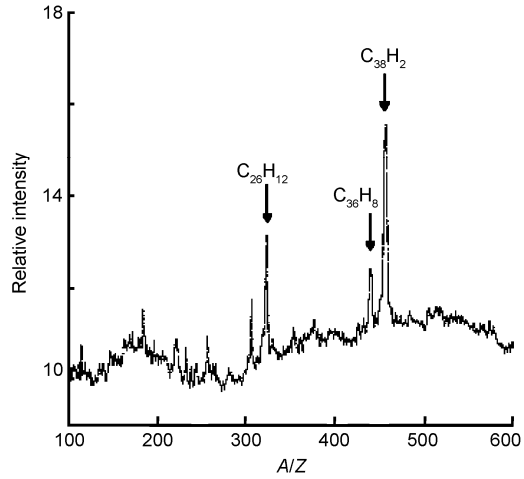

Fig.5 The TOF mass spectrum of the bombarded surface of UHMWPE.

3 Nanocrystalline diamond

It has been reported that nanocrystalline diamond films can be grown from Ar-C_{60} microwave plasma without adding molecular hydrogen to the reactant gas.[9] Fragmentation of fullerenes, especially C_2 dimer, appears to be growth species for nanocrystalline diamond.[10] Since ion bombardment can produce many C_2 dimers, we tried two ion irradiation experiments to see whether nanocrystalline diamond can be grown. The first one (Expt.1)[11,12] was to irradiate a high purity graphite plate with 0.6 keV Ar^+ ions at the fluence of $\sim 10^{22}$ cm^{-2}. The other one (Expt.2) was to apply 60 keV Ar^+ ions to irradiate the same graphite target at the fluence of 10^{19} cm^{-2}. By means of HRTEM, ED and Raman spectroscopy, we found that nanocrystalline diamond was grown in both of these two experiments.

In Fig.6, we can see that the size of diamond crystallite found in Expt.1 ranges from about 2 nm to about 70 nm while in Expt.2 from micron quantity to several nanometers. So the second experiment is more valuable than the first one at the point that large scale diamond crystallites can be synthesized and its size range is wider.

The diamond lattice fringes (see Fig.7) are distinct, and average spacing between neighboring parallel fringes is about 0.224 nm. The diamond particle shown in Fig.7 with common orientation is a perfect single crystal. In the Raman spectrum (see Fig.8) of the irradiated graphite surface in Expt.1, there are a

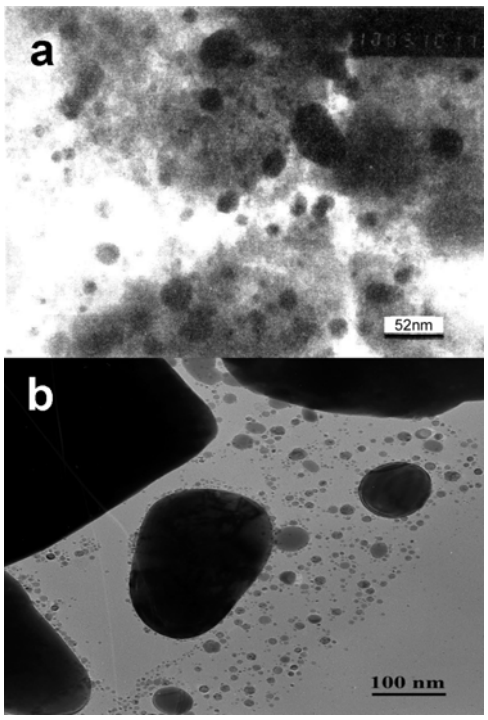

Fig.6 Low resolution TEM images of diamond particles found in Expt.1 (a) and Expt.2 (b). The dark contrast areas contain diamond nanocrystalline.

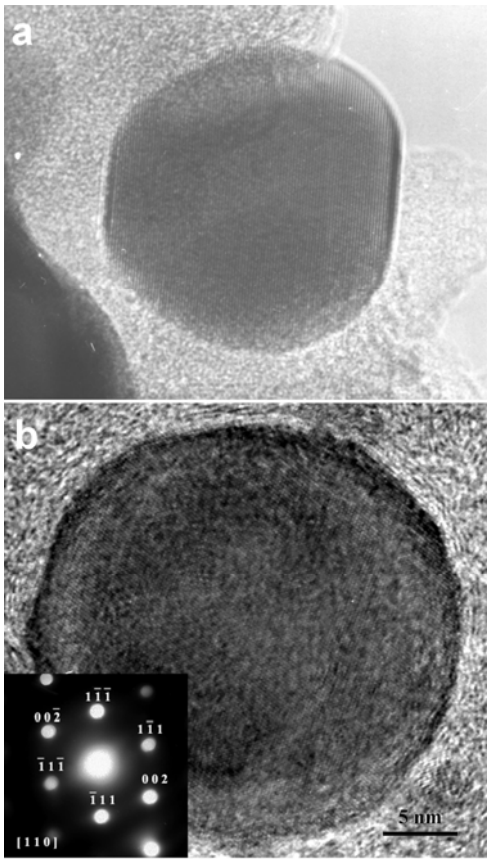

Fig.7 The HRTEM lattice image (dark contrast fringes) of diamond particles in Expt.1 (a) and that in Expt.2 with its corresponding selected area electron diffraction (SAED) patterns(b).

graphite (G-band) peak at 1581 cm^{-1} and a first-order diamond (D-band) peak centered around 1328 cm^{-1} with a FWHM of about 40 cm^{-1}. The D-line shifts downward since grain size decreases to the nanometer scale.[13] Meanwhile, the broadening of the D-line may suggest the presence of 2H and 3C cubic nanocrystalline diamond in the same micro-region of specimen since 2H and 3C cubic diamond shifting downward distances from their value of 1332 cm^{-1} for bulk diamond are different.[14,15] The ratio of peak intensities ID/IG changes its value as the probe site moves on the irradiated graphite surface (not shown here), reflecting the non-uniformity of density distribution of diamond particles with various sizes and shapes in the probe region. High ID/IG (>1) value illustrates the presence of diamond particles with nanometer size and high concentration in the probe region (as shown in Fig.8).

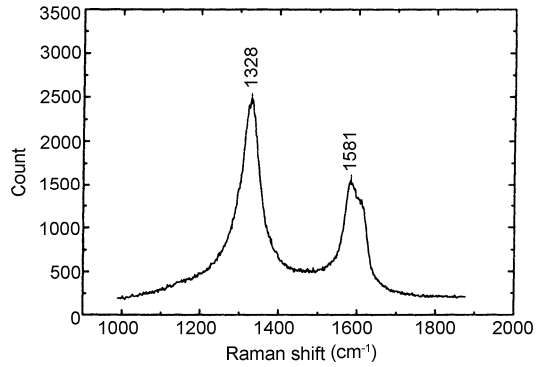

Fig.8 Raman spectrum, showing a D-peak at 1328 cm^{-1} and a G-peak at about 1581 cm^{-1}, is superimposed on a broadband centered around 1600 cm^{-1}.

4 Carbon nanotubes

Yamamoto *et al*[16] had reported that when 3 keV Ar^+ ions irradiated perpendicularly the amorphous carbon target surface at the fluence of 10^{18} cm^{-2}, there were 10- to 15-wall carbon nanotubes grown outside the irradiated area on the target surface. Since the ion track caused by irradiation was quite short, they thought that carbon nanotubes were formed when incident atoms and sputtering atoms collided with each other and then fell back on the target surface. However, it was so inconvincible because they didn't confirm directly through the experiment that these nanotubes were grown definitely outside the irradiated area and could not exclude the possibility of nanotubes grown inside the ion track area. Actually, both inside and outside of the ion track area in target material can provide the condition to form some carbon structures.[17] Once there are ion track areas formed, the carbon nanostructures such as fullerenes and nanotubes can be grown around the ion track. In order to further understand the growth mechanism of nanotubes caused by ion irradiation, we performed the experiments applying 60 keV Ar^+ ions to irradiate the graphite target also at fluence of 10^{18} cm^{-2}.[18-21]

To identify the nanostructures growth location, we introduced two ways to arrange beam and target: (1) irradiating thick graphite target (about 2 mm thick) perpendicularly, and then scraping some part in the irradiated area to examing the nanostructures grown inside the surface layers; and (2) irradiating the side surface of a thin target (about 30 μm thick) perpendicularly, and then using TEM directly to seek the nanostructures grown on the side surface or protrusion caused by ion-irradiation (see Fig.9). Bombardment of the surface with energetic ions caused various types of surface topographies, especially whisker-like protrusion structure. Recurring to the TEM, we observed many carbon polyhedrons and fullerene-like structures grown inside the irradiated surface layers (see Fig.10a), and multi-wall carbon nanotubes grown on both graphite surface layer (see Fig.10b) and whisker-like protrusions (see Fig.10c) on the surface layer.

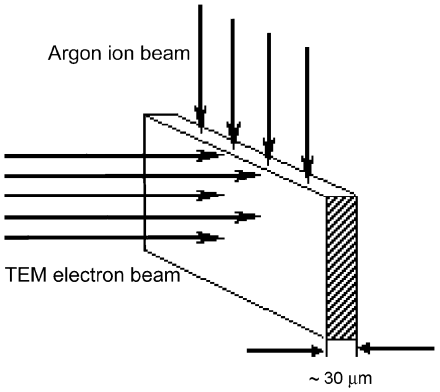

Fig.9 Schematic diagram of ion beam irradiating thin graphite plane target and its TEM analysis direction.

In our opinion, nanostructures grown on the above-mentioned three locations correspond to three different growth mechanisms. In the surface layers, the sputtered and cascade collided carbon atom plasmas possibly provide the condition for growing some nanostructures. For the nanostructures grown on the surface layer, the diffused atoms induced by ion irradiation maybe play the most important role during

their growth process. For the carbon nanotube that emerged from the whisker-like protrusion, its conical shape and smaller nanotube embedded structure suggest an open growth mechanism for it; and the source particles forming nanotube mainly come from sputtered atoms from other areas and diffused atoms on side wall of the protrusion. Because of the localization in space and discontinuity in time for ion injecting, the nanostructures appear to be terminated imperfectly and incompletely closured.

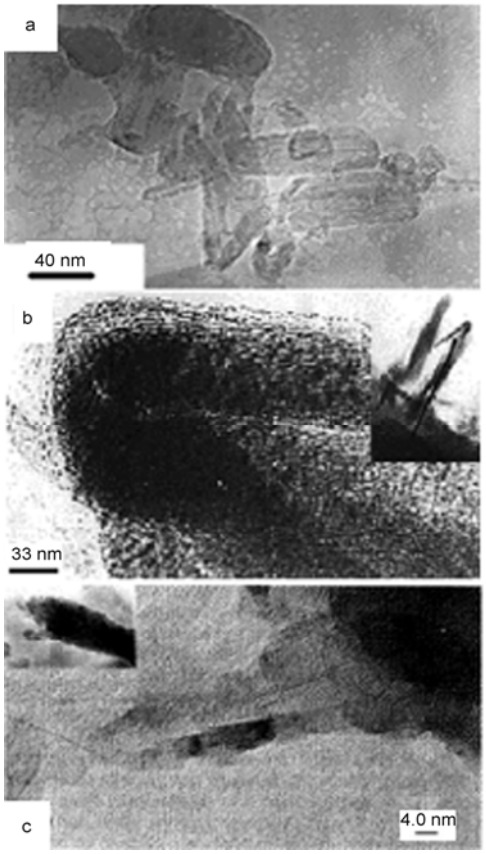

Fig.10 The TEM images of nanostructures produced by ion irradiation inside surface layers (a), on the target surface layer (b) and on the whisker-like protrusion (c).

5 Nanoscale argon-bubbles

As shown above, all the experiments are performed only with one kind of ion and without any catalyst doped in the target. In order to know what will be different if graphite target is doped with catalyst and then irradiated with ions, we carried out the following experiment.

First, we implanted Ni^+ ions as an intended catalyst into graphite target surface with 60 keV Ni^+ ions at the fluence of 10^{18} cm^{-2}. Then we employed 60 keV argon ions to irradiate this doped graphite at the same fluence under the same experimental condition. Using high-resolution transmission electron microscope (HRTEM) with energy dispersive X-ray (EDX) and electron diffraction (ED) analysis, it is very interesting to find different-size Ar-bubbles embedded in glass-carbon-like membranes for the first time.

Bubbles are composed of carbon, argon and nickel atoms and their quantity of weight is not uniform but varies with the testing areas in the ion bombarded area. Their fundus matrix is glass carbon structure suggested from the character of its electron diffraction (ED) image (see Fig.11a). These argon bubbles distribute on the graphite surface closely like an irregular honeycomb (see Fig.12). The largest bubble can be over 100 nanometers, but most of them have the diameter of about 40 to 50 nanometers. According to the gas-solid equilibrium principle on the process of bubbles growing up gradually, $P = 4\gamma/D$, where P is the argon pressure on the bubble wall, D is the average diameter of one sphere and γ is the surface tension of a hollow sphere. Referring to $\gamma = 0.01$ N for He-bubbles, and if $D = 1$ nm, argon pressure P can be estimated to be ten thousands of standard-atmosphere-pressures, and the mass density of Ar atoms in bubbles is about 1.6×10^4 kg/m^3, very close to that of solid state. Moreover, the electron diffraction on the bubble (see Fig.11b) also maybe suggest that the argon atoms in the bubble possibly be in the state of crystal.

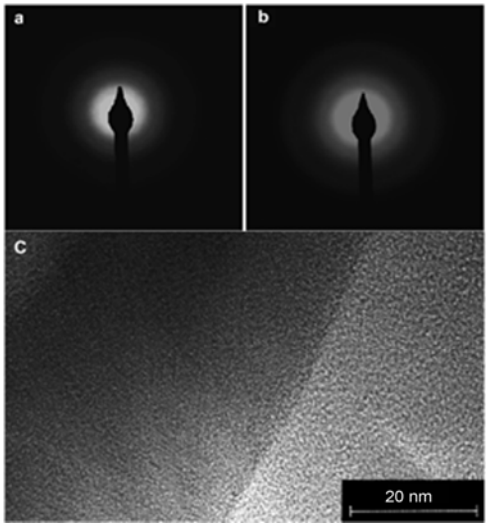

Fig.11 Electron diffraction patterns on the bubbles' fundus matrix (a) and bubble top (b), and the HRTEM image at the edge of one bubble (c).

The discovery of nanoscale argon bubbles pro-

vides us a possible novel way for growing quantum dots and enlarges the studies on quantum dots. In addition, if deuterium bubbles could be synthesized by this means, it would be a very tentative promising method to synthesize the right D-bubbles target for laser bombardment to generate nuclear fusion.

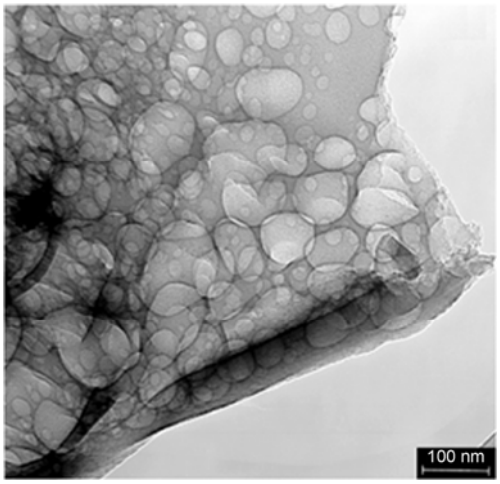

Fig.12 The HRTEM image of Ar-bubbles.

6 Amorphous carbon nanowires—welding

The structure character of amorphous carbon nanowires, a kind of polymorphic material, from short order to long order, depends on the number ratio of sp^2 to sp^3, initial carbon state and their growth methods. Charge transportation in these amorphous solid seems unusual and attractive. However, their electrical properties are still unknown and need extensive research. Anyway, we must find a way firstly to synthesize these amorphous nanowires to study their related properties. Here in the ion irradiation experiment, it is found that many of multi-wall carbon nanotubes synthesized by CVD evolve into amorphous carbon nanowires when they are irradiated by energetic ions.

The experiment was performed as the following. First, MWCNTs synthesized by CVD were spread onto a holey carbon film supported on the copper grid for TEM analysis before ion irradiation. The TEM image in Fig.13 showed that these un-irradiated hollow MWCNTs have clear crystal lattice lines of multi-wall. Second, we took out this copper grid covered with MWCNTs from TEM and then irradiated it in the magnetic isotope segregator by using C^+ ions with the energy of 40 keV at the fluence of 10^{16} cm^{-2}.

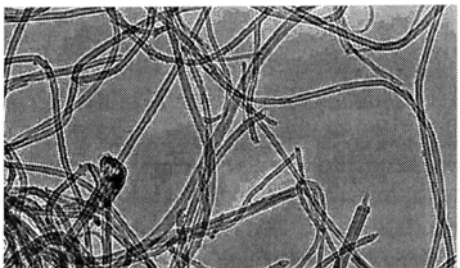

Fig.13 The HRTEM image of carbon nanotubes synthesized by CVD before ion irradiation.

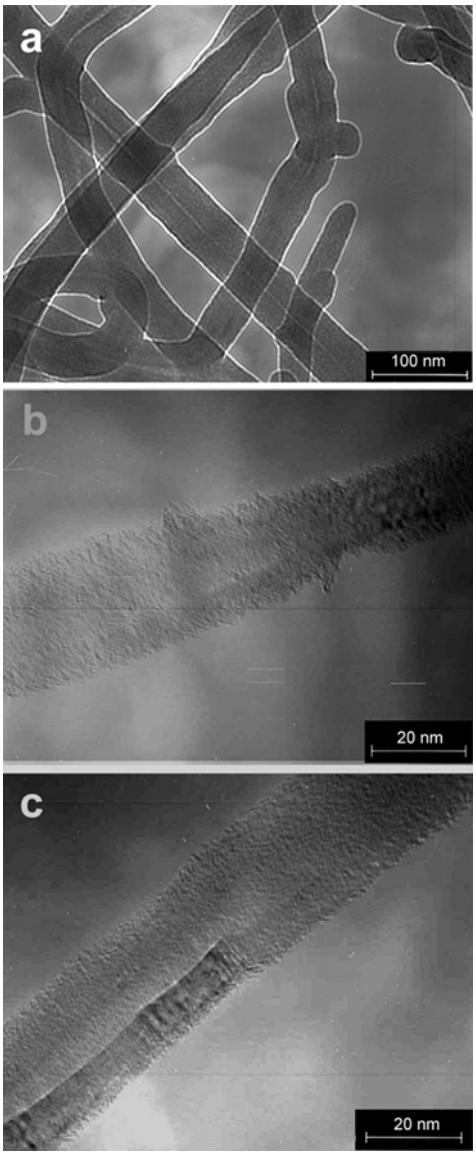

Fig.14 The HRTEM images of partly amorphous nanotubes and nanowires.

After irradiation, this grid was put into TEM for analysis once again. Most MWCNTs were found to be changed into amorphous nanowires and amorphous nanotubes (see Fig.14a). In some nanotubes, it can be

found that transitive areas of amorphous nanotubes and amorphous nanowires exist (see Fig.14c). Meanwhile, some nanotubes shrunk, and some swelled when they evolved into amorphous state (see Fig.14b). Moreover, during this evolving process, some crossed nanotubes are possibly welded together (see Fig.15), and these welded points may be found great applications in nanotube/molecular electronics.

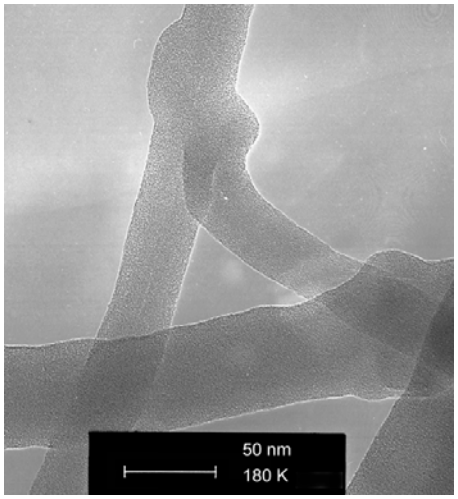

Fig.15 The HRTEM image of crossed MWCNTs.

7 Conclusion

By ion irradiation, small fullerenes C_{20} and C_{26} have been synthesized. Meanwhile, crystalline diamonds have also been produced by Ar^+ ion irradiation of graphite. On the experiment of double ions Ni^+ and Ar^+ irradiation, many nanoscale Ar bubbles formed. When multi-wall carbon nanotubes were irradiated by C^+, many MWCNTs evolved to amorphous carbon nanowires and amorphous carbon nanotubes. And there is possible welding on the crossed nanotubes.

References

1 Wang Z X, Ke X Z, Zhu Z Y *et al*. Acta Phys Sin (in Chinese), 2000, **49**: 939-942

2 Wang Z X, Ke X Z, Zhu Z Y *et al*. Phys Lett, 2001, **A280**: 351-356

3 Wang Z X, Wang W M, Zhu F Y *et al*. High Energy Phys Nucl Phys (in Chinese), 1998, **22**: 1182-1186

4 Mapelli C, Castiglioni C, Zerbi G *et al*. Phys Rev, 1999, **B60**: 12710

5 Diaz J, Martin Gago J A, Ferrer S *et al*. Diamond Relat Mater, 1992, **1**: 824

6 Ajayan P M, Ebbensen T W. Rep Prog Phys, 1997, **60**: 1025

7 Zhang Q L, O'Brien S C, Heath J R *et al*. J Phys Chem, 1986, **90**: 525-528

8 Kroto H. Science, 1988, **242**: 1139-1145

9 Gruen D M, Liu S, Krauss A R *et al*. Appl Phys Lett, 1994, **64**: 1502

10 Gruen D M, Pan X, Krauss A R *et al*. J Vac Sci Technol, 1994, **A12**: 1491

11 Wang Z X, Yu G Q, Ruan M L *et al*. Acta Phys Sin (in Chinese), 2000, **49**: 1524-1527

12 Wang Z X, Yu G Q, Ruan M L *et al*. J Appl Phys, 2002, **91**: 3480-3482

13 Ager J W, Veirs D K, Rosenblatt G M. Phys Rev, 1991, **B43**: 6491

14 Prawer S, Nugenk K W, Jamieson D N *et al*. Chem Phys Lett, 2000, **332**: 93

15 Lipp M M, Banza V G, Evans W J *et al*. Phys Rev, 1997, **B56**: 5978

16 Yamamoto K, Koga Y, Fujiwara S *et al*. Appl Phys Lett, 1996, **69**: 4174

17 Feld H, Zurmhlen R, Leute A *et al*. J Phys Chem, 1990, **94**: 1181-1221

18 Wang Z X, Zhu F Y, Wang W M *et al*. Phys Lett, 1998, **A242**: 261-265

19 Wang Z X, Zhu F Y, Wang W M *et al*. Acta Phys Sin (in Chinese), 1998, **47**: 960-964

20 Wang Z X, Zhu F Y, Wang W M *et al*. Appl Phys, 2000, **A71**: 353-355

21 Wang Z X, Zhu F Y, Wang W M *et al*. High Energy Phys Nucl Phys (in Chinese), 1998, **22**: 1182-1186